

Sparse bottleneck neural networks for exploratory non-linear visualization of Patch-seq data

Yves Bernaerts^{1,2}, Philipp Berens^{1,2,3,*}, and Dmitry Kobak^{1,*}

¹Institute for Ophthalmic Research, University of Tübingen, Germany

²International Max Planck Research School for Intelligent Systems, Tübingen, Germany

³Tübingen AI Center, University of Tübingen, Tübingen, Germany

*philipp.berens@uni-tuebingen.de, dmitry.kobak@uni-tuebingen.de

ABSTRACT

Patch-seq, a recently developed experimental technique, allows neuroscientists to obtain transcriptomic and electrophysiological information from the same neurons. Efficiently analyzing and visualizing such paired multivariate data in order to extract biologically meaningful interpretations has, however, remained a challenge. Here, we use sparse deep neural networks with a two-dimensional bottleneck and group lasso penalty to predict electrophysiological features from the transcriptomic ones, yielding concise and biologically interpretable two-dimensional visualizations. In two large example data sets, this visualization reveals known neural classes and their marker genes without biological prior knowledge.

Patch-seq is a recently developed experimental technique combining electrophysiological recordings and single-cell RNA sequencing (scRNA-seq) in the same set of neurons¹⁻⁴. Analyzing the resulting paired, or ‘two-view’, datasets remains a challenge⁵, as the dimensionality of the transcriptomic data is very high whereas the sample size is low due to the low-throughput nature of the technique.

There is a large number of linear and nonlinear methods for low-dimensional visualization of non-paired ‘one-view’ data, including principal component analysis (PCA), t-distributed stochastic neighbor embedding (t-SNE)⁶, and neural networks with ‘encoder-decoder’ architecture called autoencoders⁷⁻⁹. Autoencoder networks have been employed for the analysis of scRNA-seq data^{10,11}, showing the great potential of nonlinear parametric models for single-cell data analysis. However, very few such methods exist for low-dimensional visualizations of paired data¹². Here, we developed sparse bottleneck neural networks (sBNN) as a nonlinear framework for exploratory analysis and for obtaining interpretable visualizations of paired datasets (<https://github.com/berenslab/sparseBottleneck>).

In our architecture (Figure 1a), the sBNN compresses the high-dimensional transcriptomic data into a two-dimensional bottleneck representation via several fully-connected layers, from which one head of the network reconstructs the transcriptomic data (“autoencoder”), whereas an additional head predicts the electrophysiological properties of the neurons (“alloencoder”). We employed a group lasso penalty¹³ on the first encoding layer to enforce sparse gene selection¹⁴, followed by pruning^{15,16} of all input units except for a small predefined number (here, 25) and further fine-tuning. We also used a specialized training schedule consisting of classification-based pre-training^{17,18}, initial optimization with two frozen layers and subsequent optimization of all layers (Figure 1b, Supplementary Figures S1, S2). Note that the two-dimensional bottleneck and the group

lasso penalty are two crucial ingredients for our purpose as they allow direct visualization and interpretability, respectively.

We applied the sBNN to the two currently largest Patch-seq datasets: one dataset containing 1213 excitatory and inhibitory neurons from primary motor cortex (M1) of adult mice¹⁹ and another containing 3395 inhibitory neurons from primary visual cortex (V1) of adult mice²⁰. The electrophysiological features used to characterize the physiology of each neuron contained features such as the action potential width and amplitude or the membrane time constant (see Methods for a complete list). Together, these two datasets fully sampled the diversity of neural cell types in the neocortex^{19,20}.

To assess the predictive performance of the sBNN, we used 10-fold cross-validation (Figure 1b). For comparison, we used a linear method called sparse reduced-rank regression (sRRR)²¹ that predicts electrophysiological features from gene expression via a linear bottleneck. The cross-validated R^2 of the sRRR model with a two-dimensional bottleneck (rank-2 model) with 25 genes was 0.35 ± 0.02 (mean \pm SD across cross-validation folds) and 0.19 ± 0.01 for the M1 and V1 datasets, respectively. Without a 2D bottleneck (rank-16 model), R^2 increased to 0.40 ± 0.02 and 0.25 ± 0.01 respectively. The sBNN’s performance (with lasso penalty set to 0.1, see Methods) reached 0.39 ± 0.03 (Figure 1b, green line) and 0.26 ± 0.01 (Supplementary Figure S2c) respectively. Thus, it clearly outperformed the rank-2 linear model and performed as well as the rank-16 linear model, despite having only a two-dimensional bottleneck.

Not all electrophysiological features could be predicted equally well. For the M1 dataset, the highest cross-validated R^2 values were obtained for the upstroke-downstroke ratio of the action potential ($R^2 = 0.76 \pm 0.05$), maximum firing rate ($R^2 = 0.72 \pm 0.04$), and action potential width ($R^2 =$

0.71 \pm 0.07), whereas some other features had R^2 below 0.1 (Supplementary Figure S3).

To obtain the final model for dataset exploration and visualization, we retrained the sBNN model on the entire dataset (outside of cross-validation). For the M1 dataset, this led to the list of selected genes starting with *Sst*, *Vip*, *Pvalb*, *Gad1*, *Ndn*, *Lamp5*, etc. (genes sorted in descending order by the ℓ_2 norms of the first layer weights; Table 1), which are well-known marker genes of specific neuronal populations^{22,23}. For the V1 dataset, the list started with *Vip*, *Sst*, *Erb4*, *Cpne7*, *Pdyn*, *Nxph1*, etc. One caveat here is that our model, as any other sparse model, exhibits a trade-off between sparsity and model stability²⁴, and a slightly different set of genes can be selected upon re-training the model (see Methods and Supplementary Figure S4).

The two-dimensional latent bottleneck representation of the same sBNN model can be directly visualized in compact form together with its relationship to gene expression and electrophysiological properties (Figure 1c, d). In fact, major known groups of neurons (excitatory neurons and several families of interneurons) were well separated in the embedding for both data sets. Overlaying the selected gene expression reconstruction from the autoencoder model predictions on the latent space (Figure 1c–d, left) rediscovered well-known marker genes for these major cell families. For example, *Pvalb*, *Sst*, *Vip*, and *Lamp5* were all selected by the model for the M1 and V1 data set, and clearly distinguished specific groups of neurons in the visualization, in agreement with the literature^{22,23}. Likewise, overlaying model predictions of electrophysiological features on this embedding (Figure 1c,d, right) highlights key known properties of these major cell groups. For example, in the *Pvalb* family all transcriptomic types (different shades of red) were fast-spiking neurons with high firing rates and narrow action potentials, whereas e.g. in the *Vip* family different transcriptomic types (shades of purple) were all characterized by high input resistance, low rheobase and a propensity for rebound firing. Importantly, the sBNN extracted these major cell families, their transcriptomic signatures and their defining

electrophysiological properties from the data without any biological prior knowledge being incorporated into the model. Our sBNN also allows for meaningful biological interpretations beyond the level of major cell families: for instance for *Vip* neurons (Figure 1c, top, purple colors) we find clear separation between different t-types in the latent space, with differences in several electrophysiological properties such as the membrane time constant¹⁹.

Interestingly, selected genes beyond the known cell class markers often had direct and interpretable relations to ion channel dynamics and the predicted electrophysiological properties. For example, *Kcnc2* encodes a potassium voltage-gated channel and *Kcnip2* a calcium-binding protein directly interacting with the potassium ion channels and adapting the firing rate²⁵; the sBNN-based visualization of the M1 dataset revealed that *Kcnc2* and *Kcnip2* expression was higher in the fast spiking *Pvalb* interneurons, providing a causal hypothesis, which could be experimentally tested (Figure 1c)^{26,27}. Likewise, *Cacna1e*, selected in both the M1 and V1 dataset, encodes a voltage-sensitive calcium channel, which was more highly expressed in cell families with high afterhyperpolarization such as excitatory neurons or *Vip* interneurons²⁸.

For comparison, we provide the same kind of visualization for the linear sRRR (Supplementary Figure S5). In the first two latent dimensions for the M1 dataset, *Vip* and *Sst* populations were overlapping, despite having very different gene expression and firing properties. Indeed, only the third sRRR component separated these two families of neurons¹⁹. As sRRR is a linear model, all model predictions are linear in the embedding space (Supplementary Figure S5, left and right), in contrast to the non-linear surfaces that model predictions formed over the latent space of the sBNN (Figure 1c, left and right).

To show that sBNN framework can be used for analysis of paired data other than Patch-seq, we applied it to a CITE-seq dataset²⁹ providing a detailed multimodal characterization of cord blood mononuclear cells and in which transcriptomic and protein marker measurements are combined in the same cells. Our method could successfully predict the protein measurements from the transcriptomic data and produced biologically meaningful latent visualizations (Supplementary Figure S6), without any modifications to the training regime. For instance, the model correctly predicts high *CD4* and *CD8* protein expression in corresponding cell types (Supplementary Figure S6), while marker genes like *CD8A* and *CD8B* are being selected into the model after pruning. For the CITE-seq dataset, the sBNN strongly outperformed not only the rank-2 but also the full-rank linear sRRR model (Figure S7).

Related to our work, a coupled autoencoder framework has been recently suggested for Patch-seq data visualization^{30,31}. There, two different autoencoder networks are trained on the transcriptomic and on the electrophysiological data but are constrained to have similar latent spaces. Our

Dataset	Genes
M1	<i>Sst</i> , <i>Vip</i> , <i>Pvalb</i> , <i>Gad1</i> , <i>Ndn</i> , <i>Lamp5</i> , <i>Gm49948</i> , <i>Tac2</i> , <i>Sparcl1</i> , <i>Htr3a</i> , <i>Ndst3</i> , <i>Col24a1</i> , <i>Kcnip2</i> , <i>Plch2</i> , <i>Unc13c</i> , <i>Enpp2</i> , <i>Kcnc2</i> , <i>Gabrd</i> , <i>Galnt14</i> , <i>Dlx6os1</i> , <i>Elfn1</i> , <i>Phactr1</i> , <i>Gm11549</i> , <i>Cacna1e</i> , <i>Cplx</i>
V1	<i>Vip</i> , <i>Sst</i> , <i>Erb4</i> , <i>Cpne7</i> , <i>Pdyn</i> , <i>Nxph1</i> , <i>Pvalb</i> , <i>Mybpc1</i> , <i>Chodl</i> , <i>Egfm1</i> , <i>Cacna1e</i> , <i>Galnt16</i> , <i>Zfp536</i> , <i>Zfp804a</i> , <i>Lamp5</i> , <i>Igf1</i> , <i>Srrm4</i> , <i>Pde11a</i> , <i>Flt3</i> , <i>Nacc2</i> , <i>Akr1c18</i> , <i>Cplx3</i> , <i>Cdh7</i> , <i>Dscaml1</i> , <i>Sema5a</i>

Table 1. List of 25 selected genes for both datasets, ranked in descending ℓ_2 norm order of first layer weights.

sBNN framework is different in two ways: (i) we directly predict electrophysiological properties from gene expression levels, which is a biologically motivated choice that allows us to train a single neural network; and (ii) we use a group lasso penalty to perform a biologically meaningful gene selection.

In conclusion, we demonstrated that the sBNN framework yields compact, non-linear, and biologically interpretable visualizations of Patch-seq data. We demonstrated the value of this method using two recent Patch-seq datasets. In both cases, our method was able to separate known neuronal families and to identify prominent marker genes. Moreover, in both cases our method found ion channel genes that are directly related to electrophysiological properties, allowing to form testable hypotheses. We believe that our framework can also be applied to other kinds of multi-modal datasets in single-cell biology and beyond.

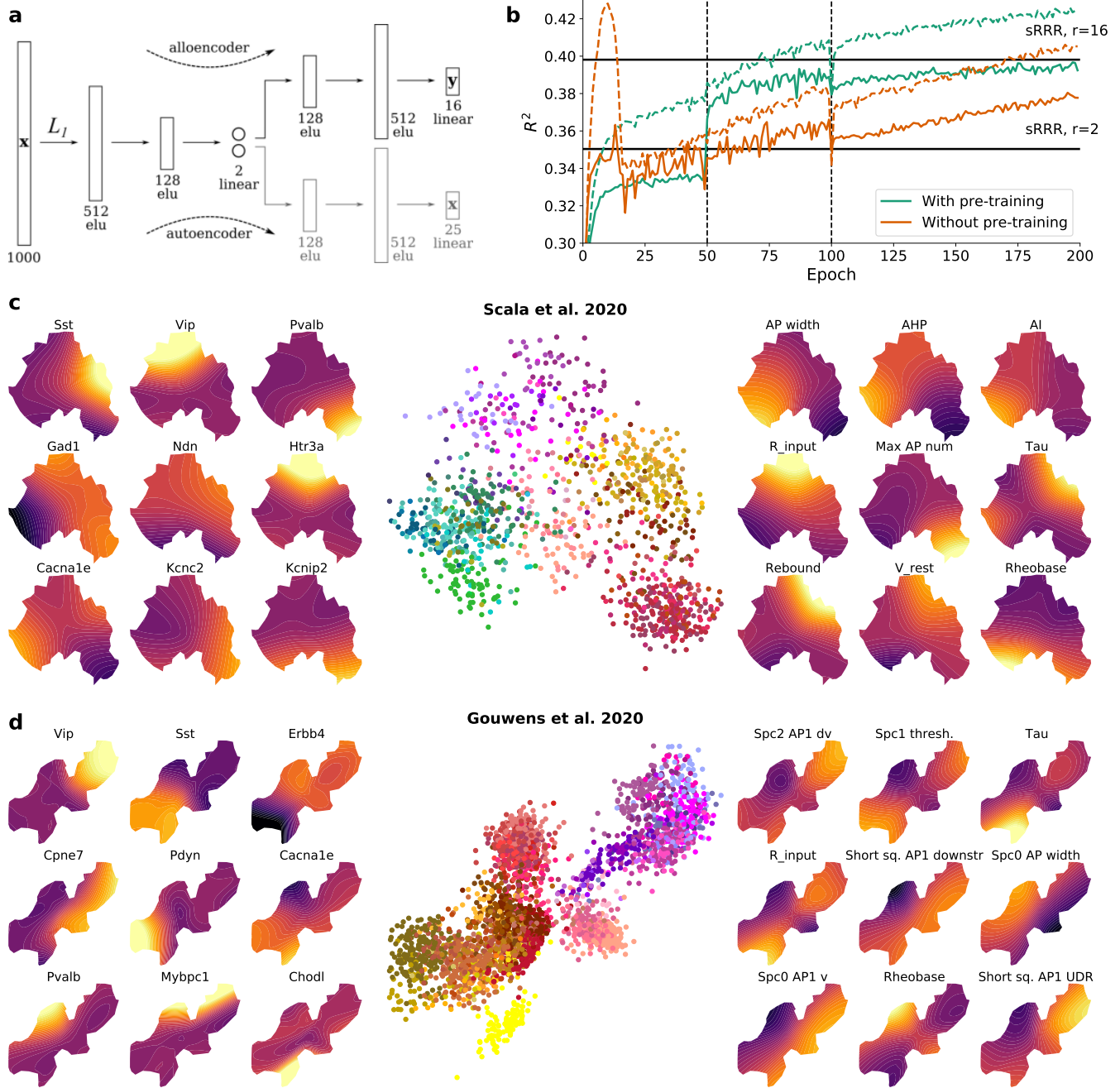


Figure 1. (a) A sparse bottleneck neural network (sBNN) schematic. Numbers denote the amount of nodes in each layer. ‘Linear’: linear units; ‘elu’: exponential linear units. (b) Training (dashed lines) and test (solid lines) R^2 of the sparse bottleneck neural network (lasso penalty 0.1). Orange lines: no pre-training. Green lines: with pre-training. The bottom two layers are frozen for 50 epochs after pre-training. All models were pruned to 25 input units at epoch 100 and trained for further 100 epochs. Horizontal lines show performances of rank-2 and rank-16 sparse RRR with 25 genes. (c) The M1 dataset. Middle: latent space of the sBNN model trained on the entire dataset (all $n = 1213$ cells are shown). Colors correspond to transcriptomic types and are taken from the original publication¹⁹. Red: *Pvalb* interneurons; yellow: *Sst* interneurons; purple: *Vip* interneurons; salmon: *Lamp5* interneurons; green/blue: excitatory neurons. Right: alloencoder model predictions for nine exemplary electrophysiological features. Left: autoencoder model predictions for nine exemplary genes out of the 25 selected genes. Model predictions were computed for all cells and the `matplotlib.pyplot.tricontourf` function was used to plot the contours on the triangulation. No smoothing was used here; network predictions were as smooth as shown. Colorscale in all overlay subplots goes from -2 (dark blue) to 2 (bright yellow). (d) The V1 dataset²⁰, $n = 3395$. Analogous to (c).

Methods

Code availability

The code in Python is available at <https://github.com/berenslab/sparseBottleneck>.

Data sources and preprocessing

The M1 data were downloaded from <https://github.com/berenslab/mini-atlas> in form of transcriptomic read counts and extracted electrophysiological features. We used the same standard³² preprocessing steps as in the original publication¹⁹. Briefly, we selected 16 well-behaved electrophysiological features (and log-transformed three of them), 1213 cells that passed the quality control and were assigned a transcriptomic type, and 1000 genes that were most variable across this subset of cells. We divided the gene counts for each cell by the cell sum over all genes (sequencing depth) and multiplied the result by the median sequencing depth size across all cells. We then log-transformed the data using $\log_2(x+1)$ transformation. Finally, all features in \mathbf{X} and \mathbf{Y} were standardized to have zero mean and unit variance. See Supplementary Figure S8 for separate visualizations of both modalities using t-SNE⁶.

The V1 data were downloaded from <https://github.com/AllenInstitute/coupledAE-patches> also in form of transcriptomic read counts and extracted electrophysiological features. This dataset²⁰ already contained normalized and log-transformed gene expression values and normalized electrophysiological feature values³¹ but for consistency we further z-scored the log-expression of all genes, excluded neurons that showed undefined electrophysiological feature values, z-scored every electrophysiological feature and excluded some of them that showed particularly high correlation with other features.

The CITE-seq data²⁹ were downloaded from <https://www.ncbi.nlm.nih.gov/geo/query/acc.cgi?acc=GSE100866> in form of transcriptomic read counts and epitomic measurements. Similarly to M1 and V1 datasets, we kept 7652 cells that were assigned a cell type specific to the immune system (excluding erythrocytes, dendritic cells and unassigned cells), all 13 epitomic features, selected 1000 most variable genes, divided the gene counts for each cell by the cell sum over all genes (sequencing depth) and multiplied the result by the median sequencing depth size across all cells. We then log-transformed the data using $\log_2(x+1)$ transformation. Finally, all features in \mathbf{X} and \mathbf{Y} were standardized to have zero mean and unit variance.

In the end, the \mathbf{X} and \mathbf{Y} data matrices had shapes 1213×1000 , 1213×16 respectively for the M1 dataset, 3395×1252 and 3395×55 for the M1 dataset and 7652×1000 and 7652×13 for the CITE-seq dataset.

List of electrophysiological features

For the M1 dataset we used the following electrophysiological features: action potential (AP) amplitude, AP ampli-

tude adaptation, AP amplitude coefficient of variation, AP threshold, AP width, afterhyperpolarization, adaptation index, interspike interval adaptation, input resistance, max AP number, membrane time constant, rebound, resting membrane potential, rheobase, hyperpolarization sag, and the upstroke-downstroke ratio. See the original paper¹⁹ for exact definitions. For the V1 dataset we refer to the original paper²⁰.

Reduced-rank regression

This paper builds on previous work suggesting to use sRRR³³ for visualization of paired datasets in genetics and neuroscience²¹. In general, RRR^{34,35} is linear regression with a low-rank constraint on the weight matrix. Its loss function can be written as

$$\mathcal{L} = \|\mathbf{Y} - \mathbf{X}\mathbf{W}\mathbf{V}^\top\|^2, \quad (1)$$

where \mathbf{X} and \mathbf{Y} are centered predictor and response data matrices, and \mathbf{W} and \mathbf{V} both have r columns, resulting in a rank- r weight matrix $\mathbf{W}\mathbf{V}^\top$. Using autoencoder terminology, \mathbf{W} and \mathbf{V} are an encoder and a decoder, respectively. Without loss of generality, it is convenient to require that \mathbf{V} has orthogonal columns, i.e. $\mathbf{V}^\top\mathbf{V} = \mathbf{I}$. RRR can be directly solved by singular value decomposition (SVD), as can be seen by decomposing its loss into the unconstrained least squares loss and the low-rank loss²¹. Regularization with a ridge penalty still allows for the direct solution using SVD.

Sparse RRR³³ imposes a group lasso penalty³⁶ on the encoder coefficients:

$$\mathcal{L} = \|\mathbf{Y} - \mathbf{X}\mathbf{W}\mathbf{V}^\top\|^2 + \lambda \sum_{i=1}^p \|\mathbf{W}_i\|_2. \quad (2)$$

Here $\sum_{i=1}^p \|\mathbf{W}_i\|_2 = \sum_{i=1}^p \sqrt{\sum_{j=1}^r W_{ij}^2}$ is an ℓ_1 norm of ℓ_2 row norms. The group lasso encourages the encoder \mathbf{W} to have sparse rows (instead of sparse individual elements), performing feature selection. It is possible to add a further ridge penalty, arriving at RRR with elastic net regularization²¹. SRRR is a bi-convex problem and can be solved by alternating steps: for fixed \mathbf{V} , the optimal decoder can be found using `glmnet`³⁷, while for fixed \mathbf{W} , the problem reduces to a Procrustes problem and can be solved using SVD^{21,36}.

Lasso and elastic net penalties can sometimes lead to over-shrinkage^{38–40} and a two-stage procedure that re-fits the model using selected predictors can lead to a higher predictive performance^{21,38,40,41}. In particular, ‘relaxed lasso’⁴⁰ fits the lasso model with some regularization parameter λ and then re-fits it using only selected predictors (i.e. predictors with non-zero coefficients) and another, usually smaller, regularization parameter λ_2 . Here we used a ‘relaxed elastic net’ variant that uses ridge penalty with the same regularization strength λ for the second-stage fit²¹. This way there is only one hyperparameter to tune.

SRRR models in this work either had rank $r = 2$ or rank $r = 16$ where rank $r = 16$ corresponded to the full dimensionality of \mathbf{Y} in the M1 dataset.

Bottleneck neural network

In our sparse bottleneck neural network (sBNN) architecture, the encoder and the decoder have two hidden nonlinear layers each (we use 512 and 128 units for the encoder, and 128 and 512 units for the decoder). We used exponential linear units for these hidden layers, but kept the bottleneck layer and the output layer linear, to match the RRR model as closely as possible (Figure 1a) and also because the response variables can take values in \mathbb{R} and are not necessarily constrained to be positive or to lie between 0 and 1. We used the mean squared error (MSE) loss function. The model was implemented using the `Keras` (version 2.2.4) and `TensorFlow` (version 1.13.1) libraries in Python.

We used a constant ℓ_2 penalty of 10^{-10} on all layers (including bias units in all layers apart from the readout layer). We found that the model performance was unaffected in a broad range of the penalty values (from 10^{-12} to 10^{-4}).

Group lasso and pruning for feature selection

To enforce sparsity, we imposed the same group lasso penalty as above on the first layer weights. This was implemented as a custom penalty in `Keras`.

The strength of the lasso penalty played an important role (Supplementary Figure S9). For low penalties such as 0.0001, the ℓ_2 weight norms for different input units before pruning were all of similar size (Supplementary Figure S9b), leading to arbitrary genes being selected after pruning and bad performance afterwards (Supplementary Figure S9a). Strong penalties (0.01–1.0) led to rapidly decaying weight norms (Supplementary Figure S9b), similar sets of genes being selected, and similar final performance (Supplementary Figure S9a), with 0.1 penalty achieving the highest performance. We used the 0.1 penalty for all models shown in Figure 1.

Linear models with lasso penalty allow for exact solutions that converge to having entries which are exactly zero³⁷. This is not the case for deep learning models, where gradient descent will generally fluctuate around solutions with many small but non-zero elements. Our strategy to achieve a genuinely sparse model was to (i) impose a strong lasso penalty and train the network until convergence; then (ii) prune the input layer by only selecting a pre-specified number of input units with the highest ℓ_2 row norms in the first layer, and deleting all the other input units; and finally, (iii) fine-tune the resulting model with lasso penalty set to zero. This procedure mimics the ‘relaxed’ elastic net procedure described above: the lasso-regularized model is pruned and then fine-tuned without a lasso penalty.

We observed a curious effect when imposing the group lasso penalty: while the training and test performance were initially both improving, after several epochs they both deteriorated rapidly (Figure S1b,c and Figure 1b, orange curve). This was not due to overfitting because the training performance became worse as well. Instead, the shape of the performance curves suggests that the lasso penalty ‘began

kicking in’, bringing the penalized MSE loss down while the unpenalized MSE loss went up. After this initial rapid decrease, the test performance slowly improved again with further training. We speculate that this behavior suggests a phase transition in the gradient descent dynamics: in the earlier ~ 10 epochs mainly the MSE (or cross-entropy) term was being optimized, while in the next ~ 10 epochs it was mainly the lasso penalty. We observed qualitatively the same phase transition when using the normal (element-wise) lasso penalty as implemented in `Keras`, so it was not specific to the group lasso penalty we used.

Training

We used the Adam optimizer⁴² with learning rate 0.0001, which we found to perform better on our dataset (possibly due to the relatively low sample sizes, see below). The default value 0.001 sometimes led to very noisy convergence, especially during pre-training (see below). All layers were initialized using the `glorot_uniform` initializer⁴³, which is default in `Keras`. The batch size for stochastic gradient descent was set to 32. It took ~ 1 minute to train any of these models for the entire 250 epochs on NVIDIA Titan Xp.

Pre-training

We performed pre-training in a classification setting with a categorical cross-entropy loss. This approach was inspired by the usual practice for image-based regression tasks to start with a convolutional neural network with weights trained for classification on ImageNet and to fine-tune them on the task at hand¹⁷. Also, it has been shown that transferring the weights from an initial task A to a target task B with subsequent fine-tuning can improve the performance on task B compared to random weight initialization¹⁸.

We used k -means clustering to cluster the whole dataset of n points into K clusters based on the values of the response variables. We then replaced the output layer of our network with a K -element softmax and trained the network to predict the cluster identity using the cross-entropy loss. This can be seen as a coarse-grained prediction because the actual \mathbf{Y} values were replaced by the cluster identities. We used $K = 20$ for all experiments.

We held out 40% of the training set as the validation set in order to perform early stopping and choose the training epoch that had the lowest unpenalized cross-entropy validation loss (during 50 epochs). We used the weights obtained at that epoch as a starting point for subsequent training with the original MSE loss. The output layer (that was not pre-trained) was initialized using the default `glorot_uniform` initializer.

A common advice in transfer learning is to hold the bottom layers frozen after the transfer (as those are the most generalizable¹⁸), train the upper layers first and then unfreeze all layers for fine-tuning⁴⁴. We tried this procedure and held the bottom two layers frozen for the first 50 epochs, and then trained the network with all layers unfrozen for

another 50 epochs. In our experiments, the performance was very similar for any number of frozen layers from two to five. We found it advantageous to reduce the learning rate after unfreezing to 0.00005 (the same learning rate was also used after pruning).

For the CITE-seq dataset we slightly modified the above procedure and used for pruning the epoch with the best validation performance after unfreezing. This was done because we observed that the network was overfitting during the 50 epochs after unfreezing (Figure S7c). However, even without this modification, the final sBNN performance was similar.

Model selection

The sample sizes of the Patch-seq datasets used in this work were very moderate by deep learning standards ($n = 1213$ for the M1 dataset and $n = 3395$ for the V1 dataset). Therefore, it was not possible to have a large test set, and evaluating performance on a small test set would yield a noisy estimate. To mitigate this problem, we used 10-fold cross-validation (CV). All models were fit 10 times on training sets containing 90% of the data and evaluated on the remaining 10%. All performance curves shown in the paper are averages over the 10 folds. The cross-validation folds were the same for all models.

We used R^2 as the performance metric for the regression models. We computed the multivariate test-set R^2 score as

$$R_{\text{test}}^2 = 1 - \frac{\|\mathbf{Y}_{\text{test}} - f(\mathbf{X}_{\text{test}})\|^2}{\|\mathbf{Y}_{\text{test}}\|^2}, \quad (3)$$

where $f(\cdot)$ is the sRRR or the sBNN output and \mathbf{X}_{test} and \mathbf{Y}_{test} were centered using the corresponding training-set means. R_{train}^2 was defined analogously. For linear models, this gives the standard expression for the R^2 (coefficient of determination). Finally, we defined test-set R^2 score for an individual electrophysiological feature i similarly as

$$R_i^2 = 1 - \frac{\|[\mathbf{Y}_{\text{test}}]_i - f_i(\mathbf{X}_{\text{test}})\|^2}{\|[\mathbf{Y}_{\text{test}}]_i\|^2}. \quad (4)$$

Training on the entire dataset

We chose the best hyperparameters and optimisation approach based on the cross-validation results, but for the purposes of visualization, we re-trained the chosen model using the entire dataset. We then passed the whole dataset through the model, to obtain the bottleneck representation, which we used for visualizations. We used the same re-trained model to analyse which features were selected into the sparse model.

Model stability

Retraining the model may yield a slightly different set of selected genes, due to randomness in the initialization and stochastic gradient descent optimization. As always in sparse models, there is a trade-off between sparsity and

model stability²⁴. Using the entire M1 dataset, we trained the same sBNN model nine more times and found that for each pair of runs, on average 14 genes were selected by both of them. 5 genes were selected 10 times out of 10: *Pvalb*, *Sst*, *Htr3a*, *Gad1* and *Ndn* (Supplementary Figure S4). Latent visualizations corresponding to different random initializations all looked qualitatively very similar and suggested the same biological interpretations (Supplementary Figure S4). Likewise, for the V1 dataset, on average 14 genes were selected for each pair of runs, and 5 genes were selected 10 times out of 10: *Pvalb*, *Vip*, *Zfp536*, *Egfm1* and *Pdyn*.

References

1. Cadwell, C. R. *et al.* Electrophysiological, transcriptomic and morphologic profiling of single neurons using Patch-seq. *Nat. Biotechnol.* **34**, 199 (2016).
2. Cadwell, C. R. *et al.* Multimodal profiling of single-cell morphology, electrophysiology, and gene expression using Patch-seq. *Nat. Protoc.* **12**, 2531 (2017).
3. Fuzik, J. *et al.* Integration of electrophysiological recordings with single-cell rna-seq data identifies neuronal subtypes. *Nat. Biotechnol.* **34**, 175 (2016).
4. Földy, C. *et al.* Single-cell RNAseq reveals cell adhesion molecule profiles in electrophysiologically defined neurons. *Proc. Natl. Acad. Sci.* **113**, E5222–E5231 (2016).
5. Liposvek, M. *et al.* Patch-seq: Past, present and future. *J. Neurosci.* (2021).
6. Maaten, L. v. d. & Hinton, G. Visualizing data using t-SNE. *J. Mach. Learn. Res.* **9**, 2579–2605 (2008).
7. Hinton, G. E. & Salakhutdinov, R. R. Reducing the dimensionality of data with neural networks. *Science* **313**, 504–507 (2006).
8. Rios, T. *et al.* Feature visualization for 3d point cloud autoencoders. In *International Joint Conference on Neural Networks*, 1–9 (Institute of Electrical and Electronics Engineers, 2020).
9. Dibia, V. & Demiralp, c. Data2vis: Automatic generation of data visualizations using sequence to sequence recurrent neural networks. In *IEEE Computer Graphics and Applications*, 33–46 (Institute of Electrical and Electronics Engineers, 2019).
10. Lopez, R., Regier, J., Cole, M. B., Jordan, M. I. & Yosef, N. Deep generative modeling for single-cell transcriptomics. *Nat. Methods* **15**, 1053–1058 (2018).
11. Eraslan, G., Simon, L. M., Mircea, M., Mueller, N. S. & Theis, F. J. Single-cell rna-seq denoising using a deep count autoencoder. *Nat. Commun.* **10**, 390 (2019).
12. Parviainen, E. Deep bottleneck classifiers in supervised dimension reduction. In *International Conference on Artificial Neural Networks*, 1–10 (Springer, 2010).

13. Yuan, M. & Lin, Y. Model selection and estimation in regression with grouped variables. *J. R. Stat. Soc. B* **68**, 49–67 (2006).
14. Zhao, L., Hu, Q. & Wang, W. Heterogeneous feature selection with multi-modal deep neural networks and sparse group lasso. *IEEE Transactions on Multimed.* **11**, 1936 – 1948 (2015).
15. Han, S., Pool, J., Tran, J. & Dally, W. J. Learning both weights and connections for efficient neural networks. In *Advances in Neural Information Processing Systems* (2015).
16. Blalock, D., Ortiz, J. J. G., Frankle, J. & Gutttag, J. What is the state of neural network pruning? In *Proceedings of Machine Learning and Systems 2* (2020).
17. Lathuilière, S., Mesejo, P., Alameda-Pineda, X. & Horaud, R. A comprehensive analysis of deep regression. *IEEE Transactions on Pattern Analysis Mach. Intell.* (2019).
18. Yosinski, J., Clune, J., Bengio, Y. & Lipson, H. How transferable are features in deep neural networks? In *Advances in Neural Information Processing Systems* (2014).
19. Scala, F. *et al.* Phenotypic variation within and across transcriptomic cell types in mouse motor cortex. *Nature Adv. online publication*. DOI: <https://doi.org/10.1038/s41586-020-2907-3> (Retrieved Nov 12, 2020).
20. Gouwens, N. W. *et al.* Integrated morphoelectric and transcriptomic classification of cortical gabaergic cells. *Cell* **183**, 935–953 (2020).
21. Kobak, D. *et al.* Sparse reduced-rank regression for exploratory visualization of paired multivariate data. *J. Royal Stat. Soc. Ser. C* (2021).
22. Tasic, B. *et al.* Shared and distinct transcriptomic cell types across neocortical areas. *Nature* **563**, 72 (2018).
23. Tremblay, R., Lee, S. & Rudy, B. Gabaergic interneurons in the neocortex: from cellular properties to circuits. *Neuron* **91**, 260–292 (2016).
24. Xu, H., Caramanis, C. & Mannor, S. Sparse algorithms are not stable: A no-free-lunch theorem. *IEEE Transactions on Pattern Analysis Mach. Intell.* **34**, 187–193 (2011).
25. Frank, A. W., Bowlby, M. R., Betty, M. *et al.* Modulation of a-type potassium channels by a family of calcium sensors. *Nature* **403**, 553–556 (2000).
26. Karsten, M., Rudy, B. & Anderson, M. Differential regulation of action potential firing in adult murine thalamocortical neurons by kv3.2, kv1, and sk potassium and n-type calcium channels. *J. Physiol.* **584**, 562–582 (2007).
27. Jiang, X., Lachance, M. & Rossignol, E. Chapter 4 - involvement of cortical fast-spiking parvalbumin-positive basket cells in epilepsy. *Prog. Brain Res.* **226**, 81–126 (2016).
28. Zaman, T. *et al.* Cav2.3 channels are critical for oscillatory burst discharges in the reticular thalamus and absence epilepsy. *Neuron* **70**, 95–108 (2011).
29. Stoeckius, M. *et al.* Simultaneous epitope and transcriptome measurement in single cells. *Nat. Methods* **14**, 865–868 (2017).
30. Gala, R. *et al.* A coupled autoencoder approach for multi-modal analysis of cell types. In *Advances in Neural Information Processing Systems*, 9263–9272 (2019).
31. Gala, R. *et al.* Consistent cross-modal identification of cortical neurons with coupled autoencoders. *BioRxiv* (2020).
32. Luecken, M. D. & Theis, F. J. Current best practices in single-cell RNA-seq analysis: a tutorial. *Mol. Syst. Biol.* **15** (2019).
33. Chen, L. & Huang, J. Z. Sparse reduced-rank regression for simultaneous dimension reduction and variable selection. *J. Am. Stat. Assoc.* **107**, 1533–1545 (2012).
34. Izenman, A. J. Reduced-rank regression for the multivariate linear model. *J. Multivar. Analysis* **5**, 248–264 (1975).
35. Velu, R. & Reinsel, G. C. *Multivariate reduced-rank regression: theory and applications*, vol. 136 (Springer Science & Business Media, 2013).
36. Yuan, M. & Lin, Y. Model selection and estimation in regression with grouped variables. *J. Royal Stat. Soc. Ser. B (Statistical Methodol.)* **68**, 49–67 (2006).
37. Friedman, J., Hastie, T. & Tibshirani, R. Regularization paths for generalized linear models via coordinate descent. *J. Stat. Softw.* **33**, 1 (2010).
38. Efron, B., Hastie, T., Johnstone, I., Tibshirani, R. *et al.* Least angle regression. *The Annals Stat.* **32**, 407–499 (2004).
39. Zou, H. & Hastie, T. Regularization and variable selection via the elastic net. *J. Royal Stat. Soc. Ser. B (Statistical Methodol.)* **67**, 301–320 (2005).
40. Meinshausen, N. Relaxed lasso. *Comput. Stat. & Data Analysis* **52**, 374–393 (2007).
41. De Mol, C., Mosci, S., Traskine, M. & Verri, A. A regularized method for selecting nested groups of relevant genes from microarray data. *J. Comput. Biol.* **16**, 677–690 (2009).
42. Kingma, D. P. & Ba, J. Adam: A method for stochastic optimization. In *International Conference on Learning Representations* (2015).

43. Glorot, X. & Bengio, Y. Understanding the difficulty of training deep feedforward neural networks. In *Proceedings of the Thirteenth International Conference on Artificial Intelligence and Statistics*, 249–256 (2010).
44. Howard, J. & Ruder, S. Universal language model fine-tuning for text classification. In *Proceedings of the 56th Annual Meeting of the Association for Computational Linguistics (Volume 1: Long Papers)*, 328–339 (2018).
45. Pedregosa, F. *et al.* Scikit-learn: Machine learning in Python. *The J. Mach. Learn. Res.* **12**, 2825–2830 (2011).

Acknowledgements

We thank Federico Scala, Andreas S. Tolias and Rickard Sandberg for discussion. This work was funded by the German Ministry of Education and Research (FKZ 01GQ1601, 01IS18039A), the German Research Foundation (EXC 2064 project number 390727645, BE5601/4-1) and the National Institute Of Mental Health of the National Institutes of Health under Award Number U19MH114830. The content is solely the responsibility of the authors and does not necessarily represent the official views of the National Institutes of Health.

Author contributions statement

YB, PB, and DK conceptualized the project. YB performed computational experiments. YB, DK and PB wrote the paper.

Declaration of interests

The authors declare no competing interests.

Supplementary figures

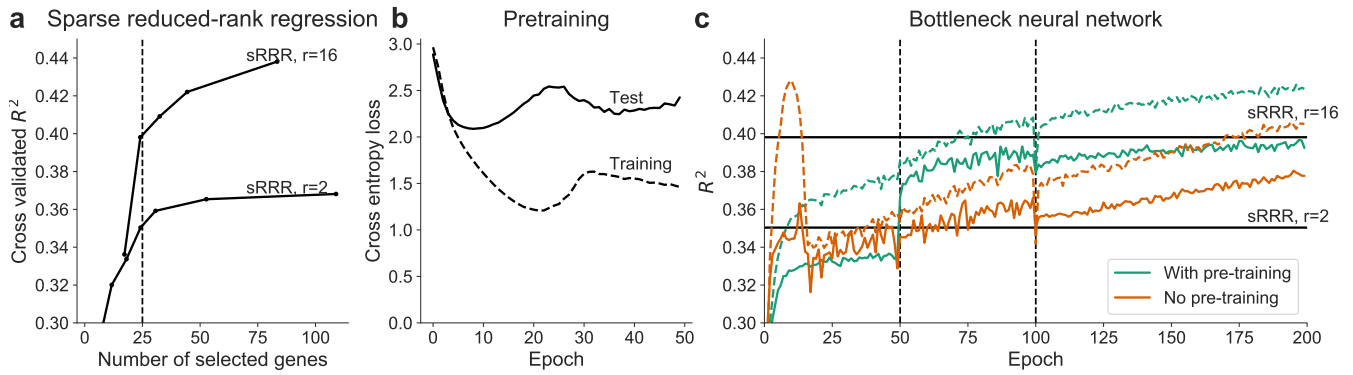


Figure S1. Linear and nonlinear sparse models, trained on the M1 dataset. **(a)** Cross-validation performance for sRRR depending on the lasso penalty that directly affects the number of selected genes (horizontal axis). Ridge regularization was set to zero. We used the ‘relaxed’ procedure, where models were re-fit using selected genes only. Lower line: rank 2; upper line: full rank (rank 16). The dashed vertical line shows the performance with 25 genes. **(b)** Training and validation cross-entropy of the pre-training phase, with lasso penalty set to 0.1. Each curve is the average over 10 CV folds. **(c)** Training (dashed lines) and test (solid lines) R^2 of the sparse bottleneck neural network (lasso penalty 0.1). Orange lines: no pre-training. Green lines: with pre-training: the bottom two layers are frozen for 50 epochs after pre-training, then unfrozen for another 50 epochs. All models were pruned to 25 input units at epoch 100 and trained for further 100 epochs. Horizontal lines show maximum performances of rank-2 and rank-16 sparse RRR with 25 genes.

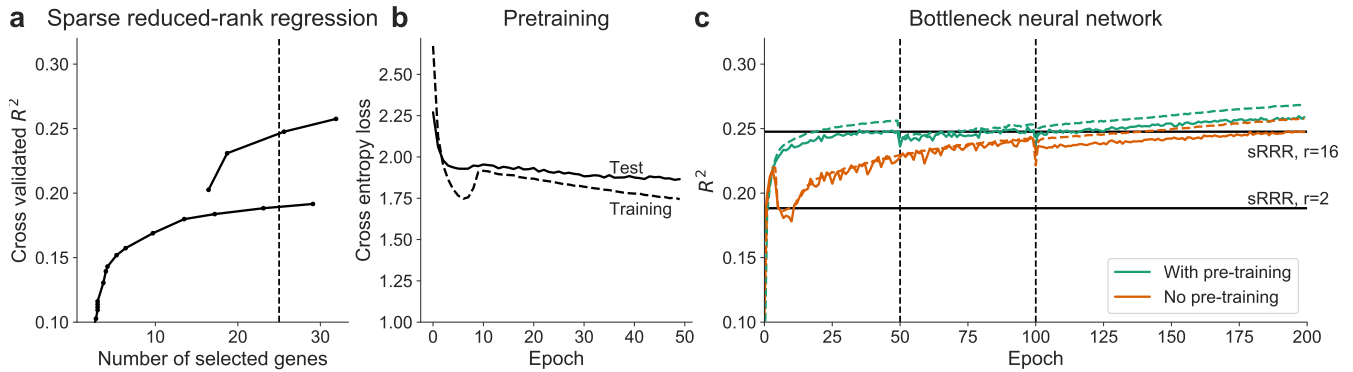


Figure S2. Linear and nonlinear sparse models, trained on the V1 dataset. Same format as in Figure S1.

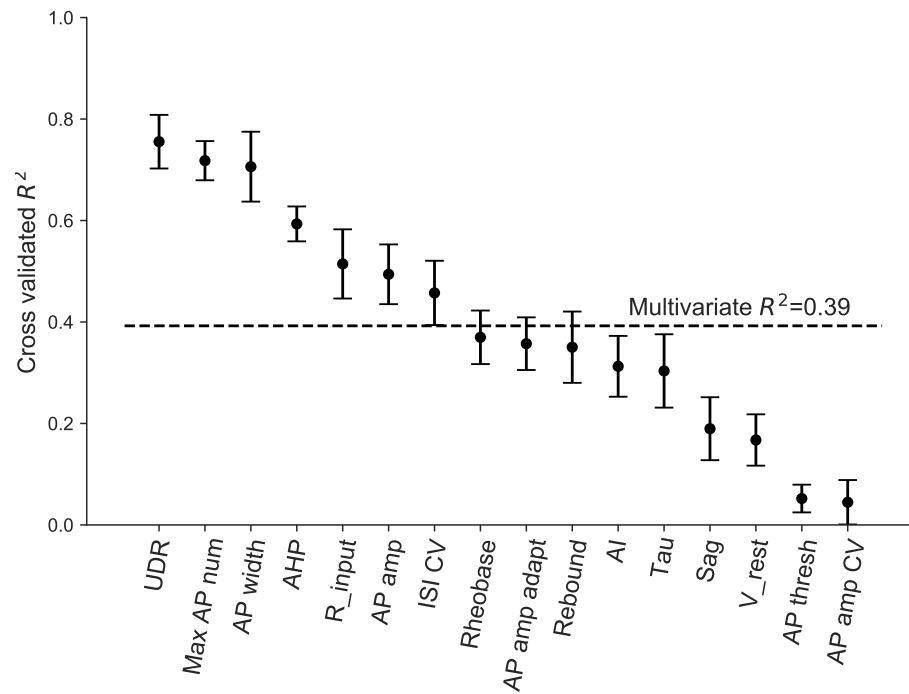


Figure S3. Predictive performance for individual electrophysiological features in the M1 dataset. Features are sorted in the order of decreasing R^2 . Error bars show \pm SD across cross-validation folds. The horizontal line shows the multivariate cross-validated R^2 score (see Methods).

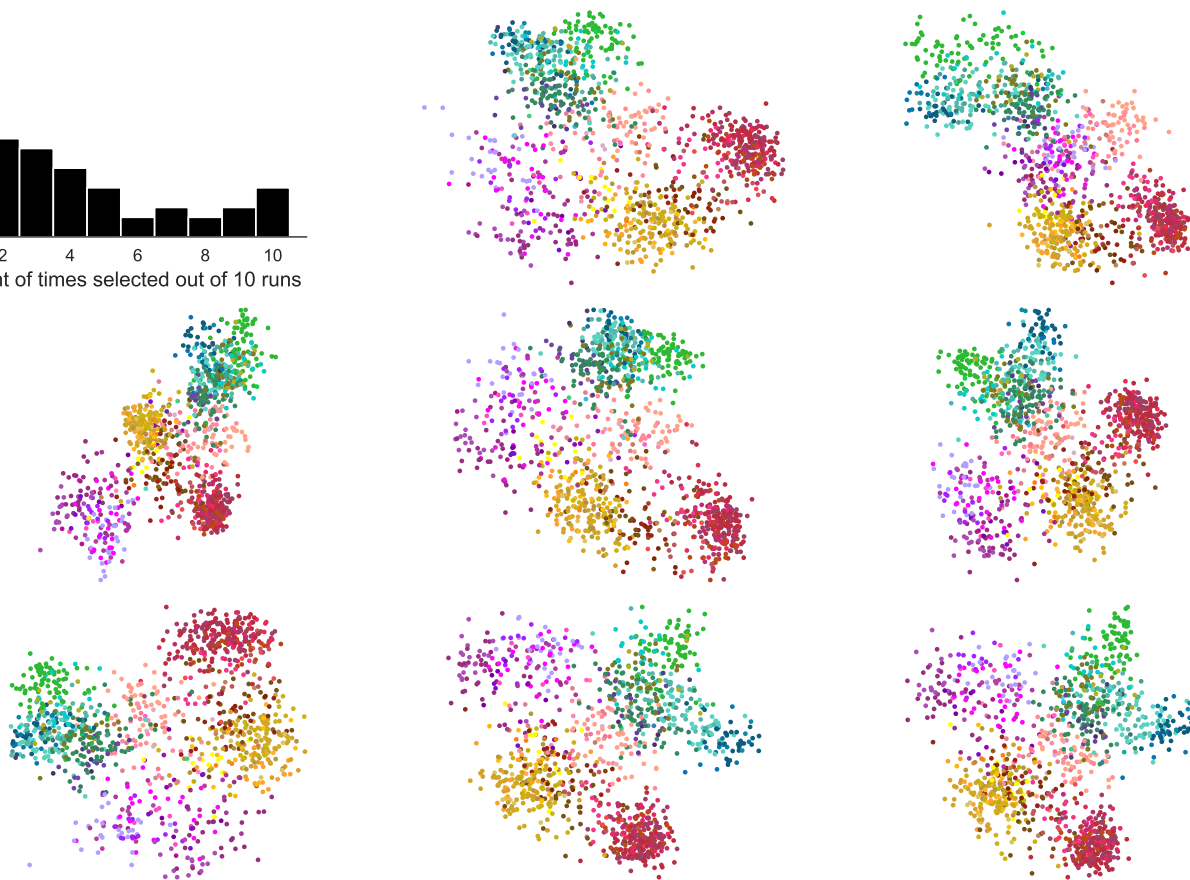
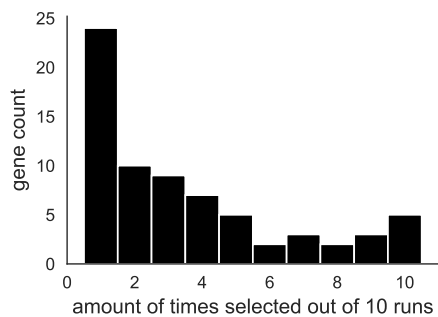


Figure S4. Model stability on the M1 dataset. **Upper left** Gene selection histogram showing how many genes were selected k amount of times in trained sBNN networks using 10 different random initializations. **Rest** Latent representations corresponding to different random initializations (8 out of 10 shown).

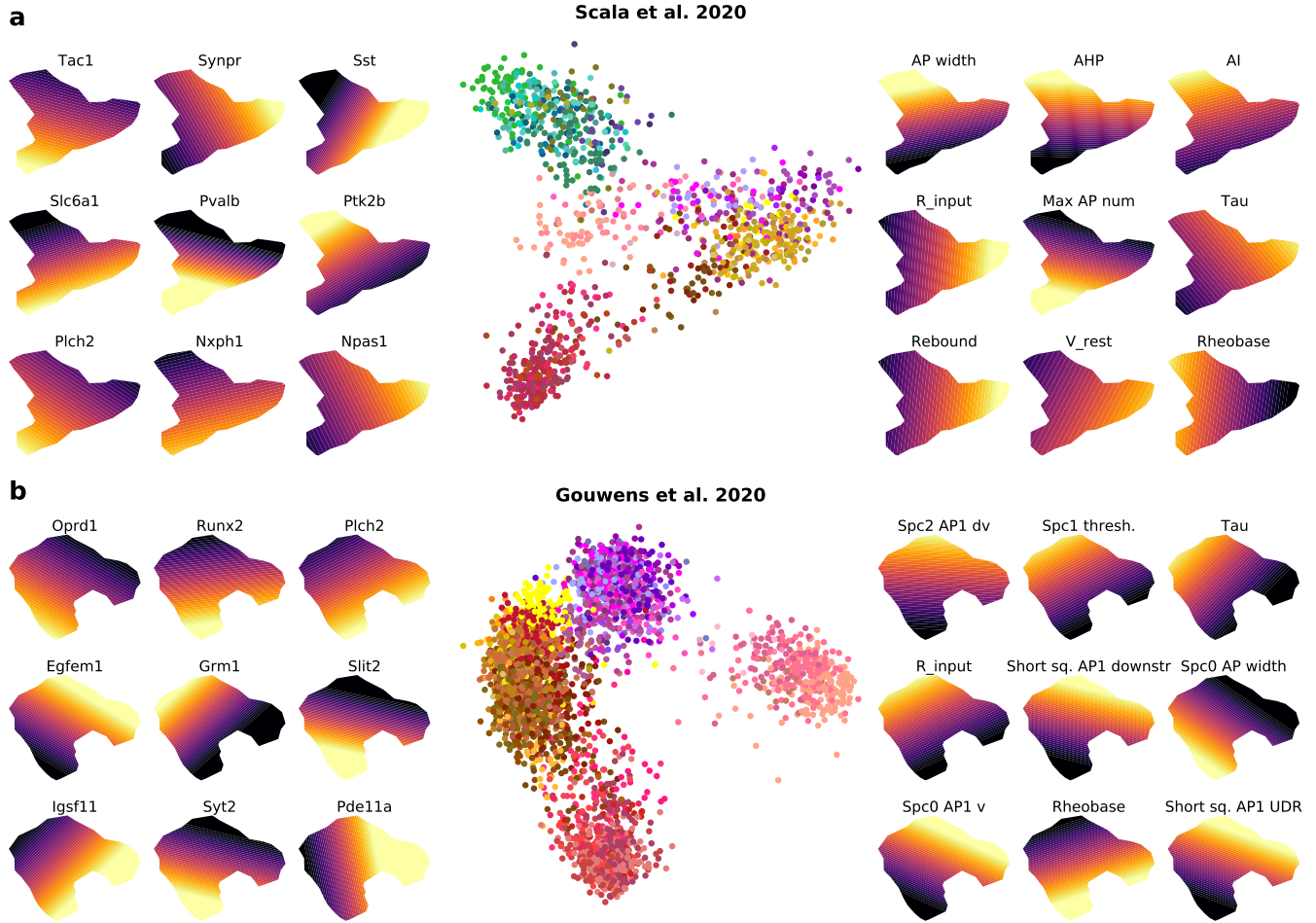


Figure S5. The latent spaces of the relaxed sRRR models trained on the M1 and V1 datasets. Colors correspond to transcriptomic types and are taken from the original publications. Red: Pvalb interneurons; yellow: Sst interneurons; purple: Vip interneurons; salmon: Lamp5 interneurons; green/blue: excitatory neurons. Colorscale in all overlay subplots goes from -1 (dark blue) to 1 (bright yellow). Same format as in Figure 1c,d. **a** M1 dataset. **b** V1 dataset.



Figure S6. sBNN analysis of the CITE-seq dataset²⁹. Sample size $n = 7652$. Same format as in Figure 1c,d. Cell identities and cluster colors were taken from the original publication. Red: CD8 T cells; green: CD16 monocytes; yellow: CD14 monocytes; blue: natural killer cells; aquamarine: CD4 T cells; magenta: B cells; brown: precursors. Colorscale in all overlay subplots goes from -2 (dark blue) to 2 (bright yellow).

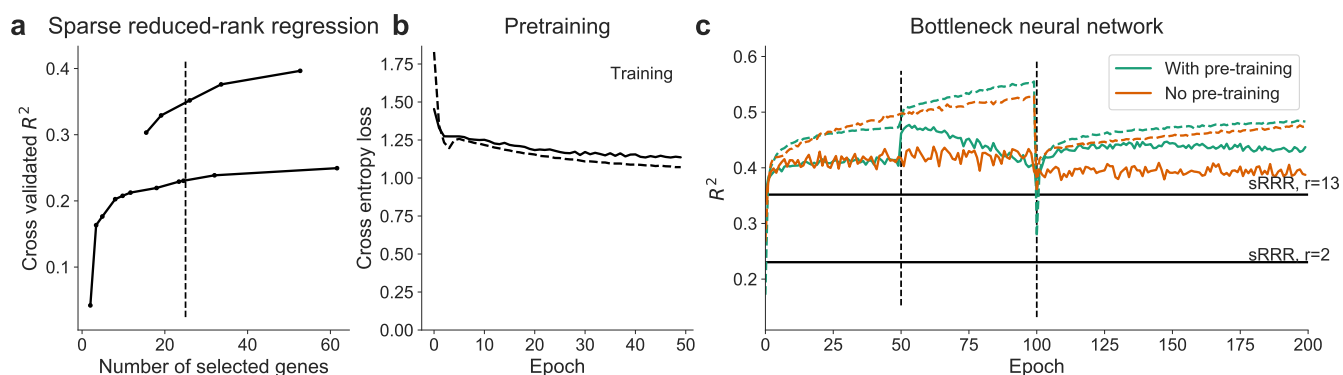


Figure S7. Linear and nonlinear sparse models, trained on the CITE-seq dataset. Same format as in Figure S1.

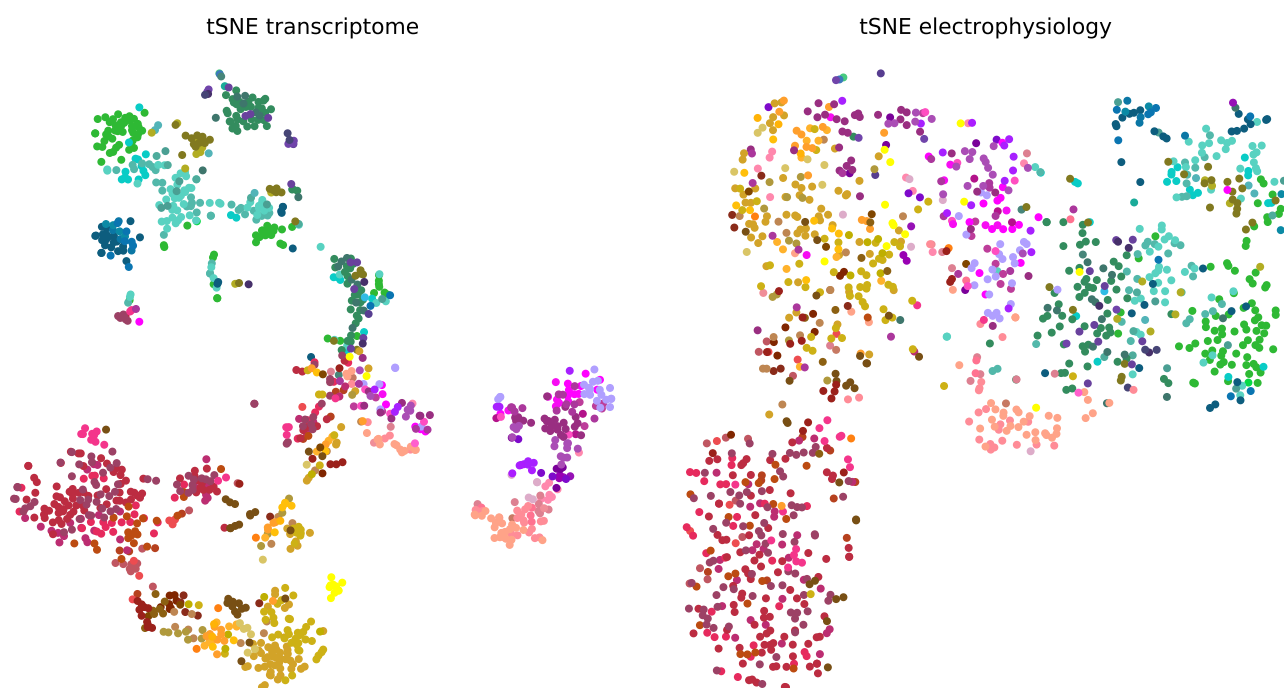


Figure S8. Separate visualizations of two modalities in the M1 dataset. **Left** T-distributed stochastic neighbor embedding (t-SNE) of the transcriptomic space. We used the `scikit-learn`⁴⁵ implementation with default parameters. **Right** t-SNE of the electrophysiological space.

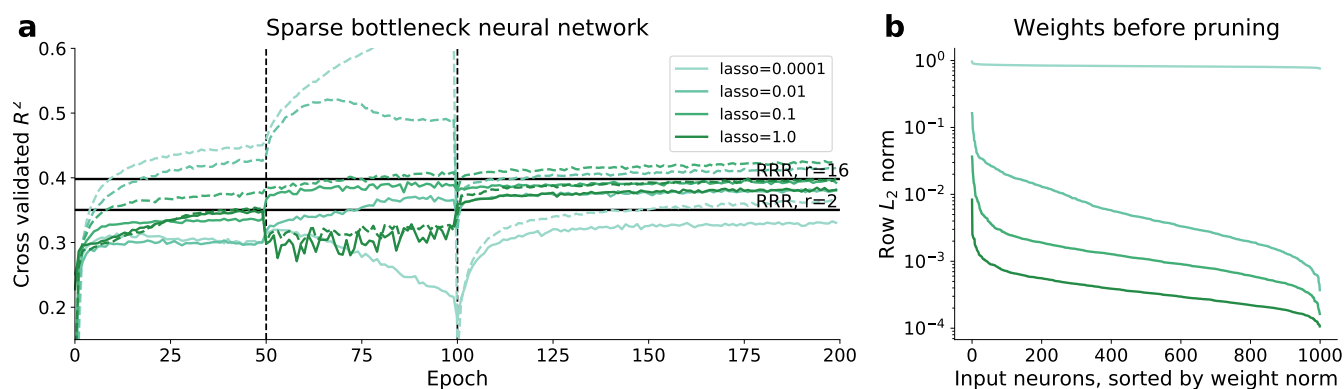


Figure S9. The effect of the lasso penalty on the M1 dataset. **(a)** Training (dashed lines) and test (solid lines) R^2 of the sparse bottleneck neural network, depending on the value of the lasso penalty (color-coded, see legend). The bottom two layers are frozen for 50 epochs after pre-training, then unfrozen for another 50 epochs. All models were pruned to 25 input units at epoch 100 and trained for further 100 epochs. Horizontal lines show maximum performances of rank-2 and rank-16 sparse RRR with 25 genes. **(b)** The ℓ_2 norms of the first layer weights for each input units just before pruning, depending on the value of the lasso penalty. These models were trained on the entire dataset. Vertical axis is on the log scale.